Publishing House
AKAPIT

COMPUTER METHODS IN MATERIALS SCIENCE

Informatyka w Technologii Materiałów

Vol. 11, 2011, No. 3

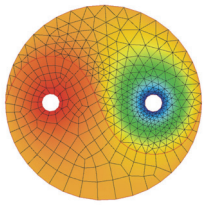

BAINITIC STEELS AS ALTERNATIVE FOR CONVENTIONAL CARBON-MANGANESE STEELS IN MANUFACTURING OF FASTENERS - SIMULATION OF PRODUCTION CHAIN

ROMAN KUZIAK[1], VALERY PIDVYSOTS'KYY[1], STANISŁAW WĘGLARCZYK[2]*, MACIEJ PIETRZYK[2]

[1]Institute for Ferrous Metallurgy, K. Miarki 12, 44-100 Gliwice, Poland
[2]Akademia Górniczo-Hutnicza, Mickiewicza 30, 30-059 Kraków, Poland
**Corresponding author: weglarcz@metal.agh.edu.pl*

Abstract

Computer aided design of the manufacturing technology for the fasteners made of bainitic steels is the objective of the paper. Main features of the new generation of bainitic steels are discussed. Rheological and microstructure evolution models for selected steel were developed. The models were implemented into the finite element code for thermal-mechanical simulations of metal forming processes. The particular objectives of the work were twofold. Simulations of various variants of manufacturing chain were performed first. Main operations, which were considered, include: hot rolling of rods and wires, cooling after hot rolling, cold drawing to reduce the diameter and forging in three operations without heat treatment. The best manufacturing chain was selected on the basis of numerical simulations. Industrial trials were performed for the selected cycle and the efficiency of this cycle was evaluated.

Key words: Bainitic steels, forging, simulation, manufacturing cycle

1. INTRODUCTION

The tendency to increase strength-to-density ratio, as well as decreasing the production costs, will be the main objectives of research on materials processing for many years. Manufacturing of high strength fasteners without heat treatment is considered in the present work. Pursuit for new steels, with higher strength, is one of the objectives of the research. Dual phase steels are one of the possibilities to reach this goal. DP steel products commercially called Dupla, which are manufactured by Corus, are available on the market. Required strength in these products is obtained without additional heat treatment. The necessity of precise controlling of cooling process after hot rolling of DP steel rods and wire rods is the disadvantage of using this material for fasteners and typically is beyond the capabilities of the Stelmor lines. The objective of the present work is searching for an alternative for manufacturing of the high strength fasteners produced without heat treating operations. This search is based on simulations of manufacturing chains.

The preliminary research described by Waengler et al. (2008) and Kuziak et al. (2011a) have shown that new generation bainitic steels can be considered for this purpose. These steels are characterized by high strength properties and reasonably good ductility (Bhadeshia & Edmonds, 1980), what creates wide possibilities of their applications. Kuziak et al. (2009) describe general aspects of modelling of closed die forging of bainitic steels. Present paper is focused on manufacturing of fasteners made of these steels.

Earlier research (Madej et al., 2009b; Kuziak et al., 2011a; 2011b) focused on the final processes of

 ISSN 1641-8581

cold drawing and forging. The present work is a continuation of (Kuziak et al., 2011a) works and simulations of the whole manufacturing chain are performed. The chain is composed of hot rolling of rods or wires, cooling after rolling, cold drawing and multi step cold forging. The methodology of simulation of manufacturing chains proposed by Madej et al. (2007) and applied to the connecting parts by Pietrzyk et al. (2008), is used.

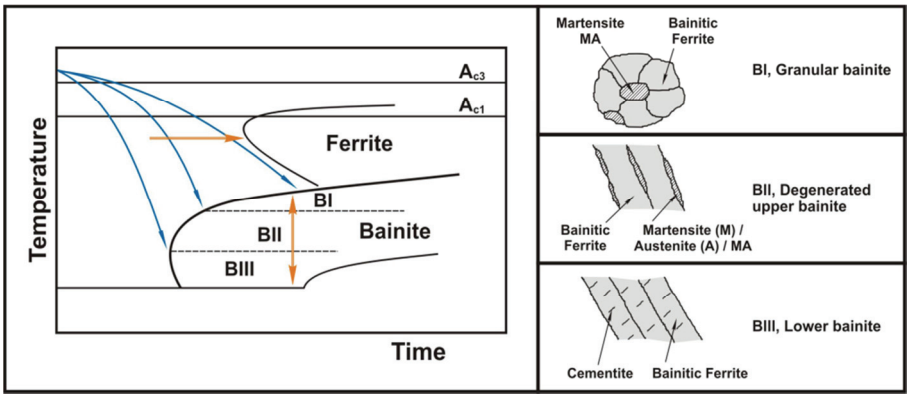

Fig. 1. *Classification and conditions for occurrence of morphological types of the bainite: granular bainite (BI), degenerated upper bainite (BII) and lower bainite (BIII).*

2. BAINITIC STEELS

Classical bainite is defined as micro-composite composed of bainitic ferrite and carbides, resulting from the austenite decomposition, which precipitate in a non-coordinated way together with the ferrite. Bainitic transformation combines features of diffusive and non-diffusive (controlled by slip) transformations (Bhadeshia & Edmonds, 1980). Lack of coordination causes that in the initial phase of the transformation bainitic ferrite is created and, after that, the remaining austenite becomes richer in carbon and is decomposed into carbides and low temperature transformation products. In this Chapter, the morphological types of bainite, which are suitable for manufacturing cold forging products, are discussed.

2.1. Morphological types of bainite

Originally two morphological types of bainite were distinguished, namely, upper and lower bainite. However, invention of the incomplete austenite transformation resulted in the change in understanding of the mechanisms of bainite formation. The bainite is now defined as microstructure composed of bainitic ferrite and hard phase components with hardness much higher than that of the bainitic ferrite. Figure 1 shows an example of modern classification of morphological types of bainite.

Beyond the two main types of the bainite (upper and lower), classification in figure 1 distinguishes additionally degenerated upper bainite and granular bainite. In both these types of bainite, the layers or particles composed of austenite and martensite are the hard component of the bainite (MA component). The term degenerated means that the microstructure contains products of incomplete austenite transformation. Zajac et al. (2005) have shown that, depending on the chemical composition and on the conditions of heat treatment, the hard component in bainitic steels can have various morphological forms, which were not considered earlier. Ranges of the temperature, in which various morphological types of the bainite become dominating, are presented in figure 1, as well. Research performed by the Authors of the present work have shown that the granular bainite without precipitates of the cementite is the most advantageous morphological type for products manufactured by forging. This morphological type of the bainite is characterized briefly below.

2.2. A granular bainite

A granular bainite occurs in the high temperature range of the bainitic transformation, directly below the start temperature Bs for this transformation. Only carbon segregates during the transformation and local equilibrium is observed at the interface (figure 2). This leads to a steep gradient of the carbon concentration in the remaining austenite and, in consequence, to the differentiation of the products of subsequent transformations in its volume. In particular, high carbon concentration close to the interface can cause stabilization of the austenite in this area. An example of such structural component in the CrNiV bainitic steel is show in figure 3. This component is composed of the outer layer of the retained austenite and bainitic ferrite with particles of cementite and, probably, some martensite inside the grain. For low carbon concentration in steel the austenite is transformed into phases characterised by high ductility. Such morphology of the hard component gives high workability during cold forming. Further increase of the workability can be obtained by a decrease of the size of the hard particles in the granular bainite, which can be obtained by thermo-mechanical rolling.

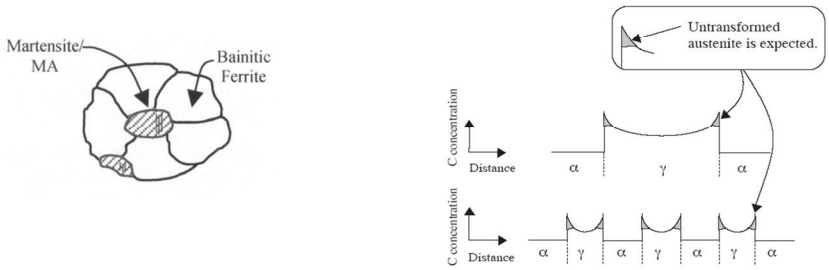

Fig. 2. *Characteristic of the morphology and mechanism of occurrence of the granular bainite.*

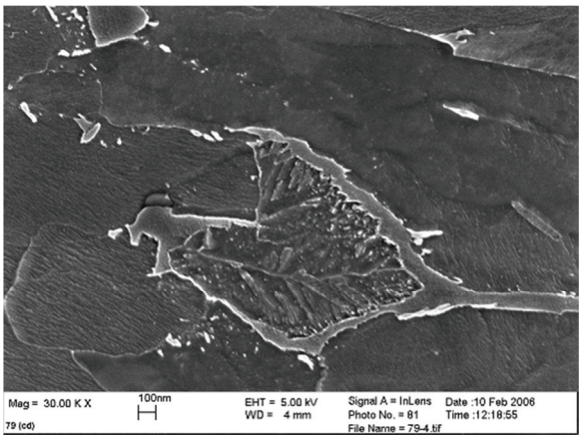

Fig. 3. *Granular bainite in the CrNiV steel; FEM-SEM.*

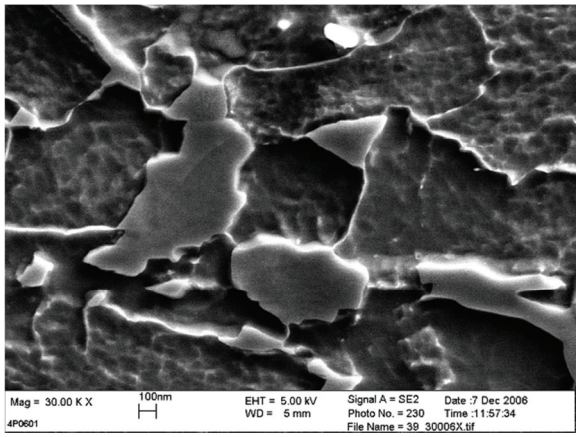

Fig. 4. *Microstructure of the granular bainite in the NiTiB steel, in which MA particles are the hard components; FEG-SEM.*

Thus, the granular bainite is usually a mixture of irregular grains of the bainitic ferrite and hard particles, which are composed of martensite and retained austenite. Microstructure of the granular bainite in the NiTiB steel is shown in figure 4. Dislocation density in the bainitic ferrite is about two orders higher than in the allotriomorphic ferrite. Ferrite with such morphological features is called quasi-polygonal ferrite. Lack of cementite is a desired feature of the granular bainite. However, during cooling austenite enriching in carbon can be decomposed into more complex morphological components, which composition and morphology depend on the alloying elements in steel.

According to Zajac et al. (2005) the hard component of the granular bainite can occur as:

- Degenerated pearlite or cementite. This morphology develops in a steel characterized by a low hardenability and is characteristic for steels with alloying elements, which decrease activity of carbon in the solid solution, eg. molybdenum. Cementite is one of the products of decomposition of rich in carbon austenite. The products of the decomposition are distributed not uniformly with cementite particles precipitating along the grain boundaries. In consequence, this morphological type is not suitable for cold forming and is not discussed further in the present paper; see Zajac et al. (2005) for more information.
- Composite martensite–high carbon bainite. When the cooling rate increases, the rich in carbon austenite is decomposed into large number of particles of cementite. When the precipitation of the cementite is stopped, MA particles occur in the bainite. This morphological type is not discussed in the present paper, either.
- Mixture of products of incomplete austenite transformation. The alloying elements, which increase activity of carbon, eg. nickel, involve decrease of the rate of the γ-α transformation and can even stop this transformation. For low cooling rates the retained austenite can be transformed into microstructure composed of fine, irregular grains of ferrite, cementite and MA particles. This microstructure exists either as fine grains in the neighbourhood of the bainitic ferrite or as part of large grains of bainitic ferrite, in their corners. Microstructure of the granular bainite in a steel NiCrV, in which the hard components are bainite, martensite and irregular mixture of products of uncompleted transformation, is shown in figure 5.
- Composite martensite–austenite. MA particles are the most common hard components in bainitic steels (figure 4). They usually

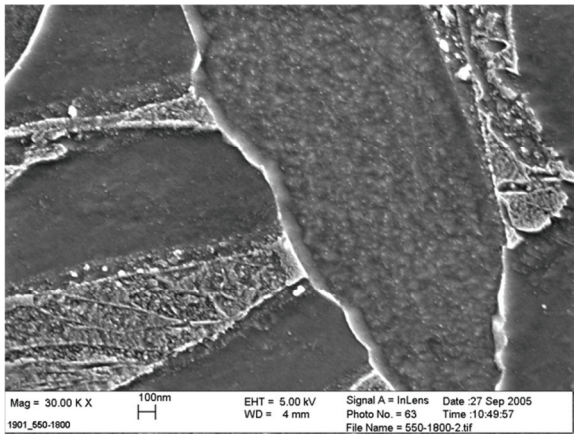

Fig. 5. *Microstructure of the granular bainite in the steel NiCrV, in which the hard components are bainite, martensite and irregular mixture of products of uncompleted transformation; FEG-SEM.*

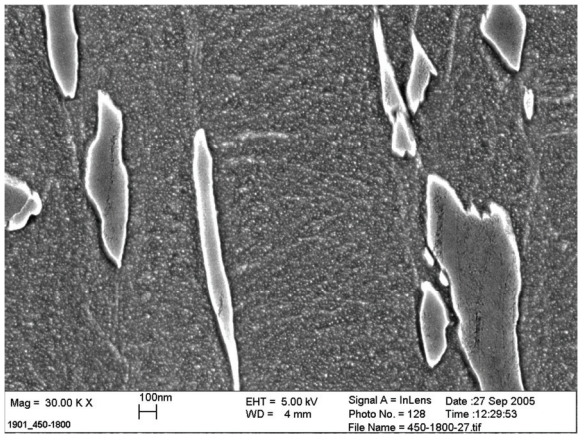

Fig. 6. *Microstructure of the granular bainite in the steel NiCrV, in which the hard components are martensite and micro composite MA; FEG-SEM.*

Table 1. *Chemical composition (wght %) of the investigated steel.*

C	Mn	Si	Al	Cu	Nb	Ti	P	S	B	N
0.074	2.0	0.28	0.034	0.10	0.038	0.13	0.012	0.011	0.002	0.0038

exist either in the form of small islands between grains of the granular ferrite or as layers at boundaries of large grains encompassing incomplete austenite transformation products, which is a product of decomposition of the outer layer of remaining austenite after bainitic ferrite development characterized by a higher carbon content (figure 2). Examples of hard MA particles are shown in figures 4 and 6. The difference between the two photos is that in figure 6 the grains of the bainitic ferrite and hard components are strongly elongated. It can be concluded that it is a transient form between granular bainite and upper bainite.

- Martensite. For high carbon content in steel, when thermo-mechanical treatment is applied, martensite may be the only hard component in the granular bainite.

Recapitulating, the morphology presented in figure 4, characterized by small and uniformly distributed MA particles in the bainitic ferrite matrix, is the most suitable for cold forming. It contains bainitic ferrite with small MA particles. The morphology presented in figure 3 is the next alternative. In this morphology the second phase has complex structure composed of outer layer of the retained austenite and products of not completed austenite decomposition located in the centre.

2.3. Selection of the material and laboratory tests

Several bainitic steels with various chemical compositions have been tested and a steel with the chemical composition given in table 1 has been selected for the further analysis. All the models, which were developed in this work, were identified for this selected steel.

The samples used in all cold forming simulations were obtained from hot rolled rods or wires. Two finishing rolling temperatures (980°C and 800°C), giving different microstructure and properties, were applied. These samples are referred to as B1 and B2, respectively. The objective of the laboratory tests was analysis of the microstructure evolution at various stages of the manufacturing chain and supplying data for models identification. The tests included:

- Physical simulation of hot rolling using the Gleeble 3800 simulator;
  - Physical simulation of cooling after hot rolling;
  - Hot plastometric tests;
  - Cold plastometric tests;
  - Dilatometric tests;
- Physical simulation of cold forging.

Physical simulation of hot rolling and cooling was performed for various finishing rolling temperatures (T_{fr} = 980°C and 800°C) and various finish temperatures for the accelerated cooling (T_{fc} = 400°C-550°C). Accelerated cooling with the rate of 10°C/s was applied. Selected results of measurement of mechanical properties after various cooling schedules are shown in figure 7.

Microstructure of all samples was investigated using optical microscope, high resolution scanning microscope (FEG_SEM) and EBSD technique.

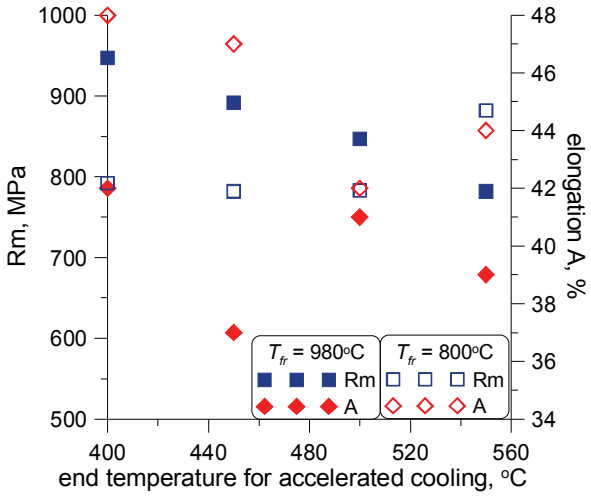

Fig. 7. *Properties of the bainitic steels depending on the finishing temperature in hot rolling and for various finish temperatures for the accelerated cooling.*

a)

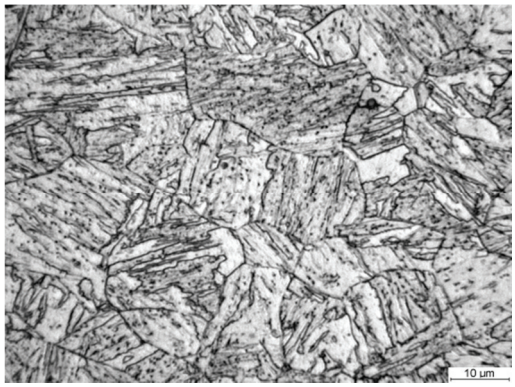

b)

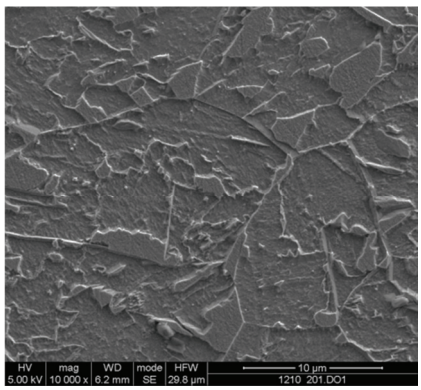

Fig. 8. *Microstructure of the bainitic steels for the finishing rolling temperature 980°C and finish of accelerated cooling temperature 550°C, a) optical microscopy, b) FEG SEM.*

Samples deformed with the finishing temperature T_{fr} = 980°C are fully recrystallized with the grain size of 25-30 µm. In these samples, lower T_{fc} gives higher strength with maintained high plasticity. T_{fc} = 550°C gives granular bainite microstructure, with large tough particles located at the austenite grain boundaries, which cause decrease of the plasticity (figure 7). Microstructures for T_{fr} = 980°C and T_{fc} = 550°C are shown in figure 8.

a)

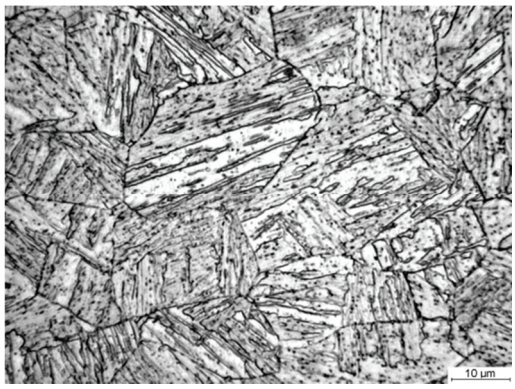

b)

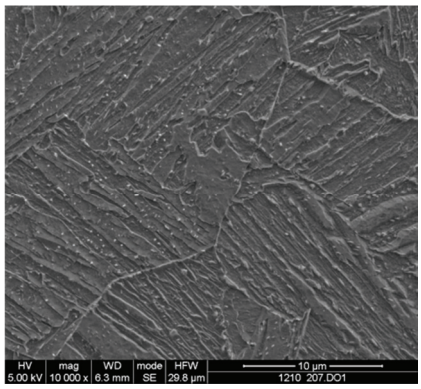

Fig. 9. *Microstructure of the bainitic steels for the finishing rolling temperature 980°C and finish of accelerated cooling temperature 400°C, a) optical microscopy, b) FEG SEM.*

Lower T_{fc} (500-450°C) gives increased volume fraction of upper and lower bainite and decrease of the volume fraction of the granular bainite. Some self tempered martensite is observed along with the upper and lower bainite for T_{fc} = 400°C. Microstructures for T_{fr} = 980°C and T_{fc} = 400°C are shown in figure 9. Results of the scanning microscopy show that the hard component of the structure is nonuniformly distributed and it is composed of tempered martensite, retained austenite, high carbon bainite and, eventually, irregular mixture of ferrite and cementite. Micrographs allow also to conclude that simultaneous increase of strength and ductility after accelerated cooling may be due to gradual decrease of the size of hard particles. Increased plasticity for lower T_{fc} is due to the decrease of the size of hard particles.

After the deformation at 800°C static recrystallization of austenite is totally suppressed due to the dynamic precipitation of TiC. This promotes occurrence of the allotriomorphic ferrite, which is one of the reasons of discrepancies in properties of samples

for various finishing rolling temperatures. Due to occurrence of this ferrite, the strength of the samples deformed at 800ºC is lower compared to the one deformed at 980ºC. Beyond this, there is no significant effect of the T_{fc} temperature on the strength of the samples deformed at 800ºC (figure 8). Selected microstructures of the samples deformed at 800ºC are shown in figures 10 and 11.

a)

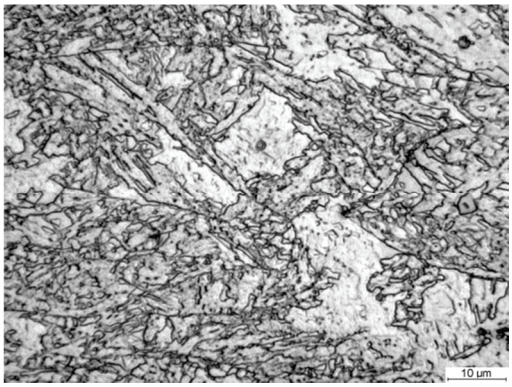

b)

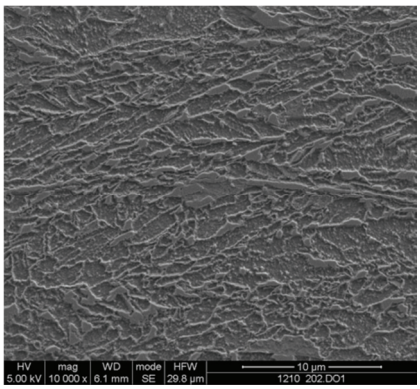

Fig. 10. *Microstructure of the bainitic steels for the finishing rolling temperature 800°C and finish of accelerated cooling temperature 550°C, a) optical microscopy, b) FEG SEM.*

Dilatometric tests were carried out for various cooling rates. Two sets of the tests were performed. In the first set the procedure included preheating at 1200°C for 600 s, cooling to 1000°C, plastic deformation at this temperature and further slow cooling to 850°C followed by controlled cooling with various cooling rates. In the second set of the tests the plastic deformation was applied at 870°C. The dilation curve was monitored and start and end temperatures for phase transformations were calculated for all the tests. Volume fractions of structural components at room temperature were measured, as well. All these data were used as an input for the inverse analysis, which was performed to identify the parameters in the phase transformation models. Beyond this, the microstructure of samples before and after cooling was investigated.

a)

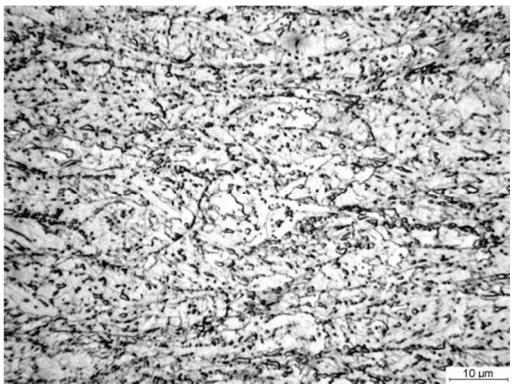

b)

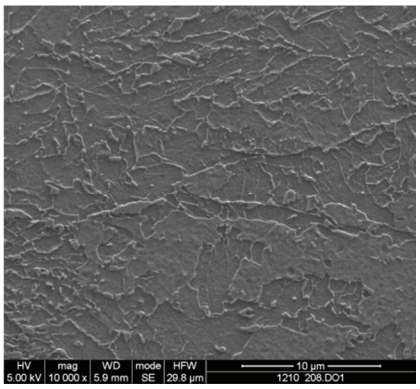

Fig. 11. *Microstructure of the bainitic steels for the finishing rolling temperature 800°C and finish of accelerated cooling temperature 400°C, a) optical microscopy, b) FEG SEM.*

At the beginning of the phase transformation microstructure of the samples deformed at 1000°C was fully recrystallized and the average grain size was about 30 µm. Microstructure of the samples deformed at 870°C was not recrystallized, grains were elongated and the average grain size was about 45 µm. It was observed that conditions of the tests have strong influence on the microstructure of the investigated steel. Selected microstructures are presented in figures 12 and 13. The following correlations between cooling rate (C_r) and structure were noticed:

- $C_r < 1$°C/s – ferrite, pearlite and granular bainite,
- 1°C/s < C_r < 6°C/s – ferrite, granular bainite, upper bainite and martensite,
- $C_r > 6$°C/s – ferrite (traces), upper and lower bainite and martensite.

Beyond this, performed tests allowed following conclusions:

- Deformation below the recrystallization temperature promotes the occurrence of the granular bainite, see figure 12b.

a)

b)

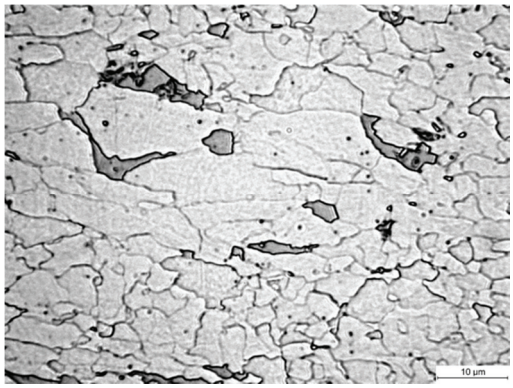

Fig. 12. Microstructure of the bainitic steels deformed at 1050°C (a) and 870°C (b) and cooled with the rate of 1°C/s.

a)

b)

Fig. 13. Microstructure of the bainitic steels deformed at 1050°C (a) and 870°C (b) and cooled with the rate of 6°C/s.

- In non recrystallized austenite ferrite occurs at higher cooling rates comparing to the recrystallized austenite.
- For low cooling rates ($C_r < 2$°C/s) granular bainite is characterized by relatively large grain size and large dimension of the hard component, which is nonuniformly distributed in the steel structure. It means that cooling rate after hot rolling should be in the range 3-6°C/s. This cooling rate can be easily reached in the Stelmor system.
- Accelerated cooling should be finisher at the temperature of 400-450°C.

Objectives for the optimization of the manufacturing chain were formulated having above conclusions in mind.

3. MODELS

All simulations were performed using Forge 3 finite element (FE) software. Rheological model and finite element model are described briefly below. Microstructure evolution model developed for the bainitic steels, which is described below as well, was implemented in the FE code.

3.1. FE model

Forge 3 software is based on the Norton-Hoff viscoplastic flow rule. This rule was originally introduced by Norton (1929) for one-dimensional creep. It was extended by Hoff (1954) to three dimensions. The main equation of this law is:

$$\boldsymbol{\sigma} = 2K\left(\sqrt{3}\dot{\varepsilon}_i\right)^{m-1}\dot{\boldsymbol{\varepsilon}} \tag{1}$$

where: $\boldsymbol{\sigma}$, $\dot{\boldsymbol{\varepsilon}}$ – stress and strain rate tensor, respectively, $\dot{\varepsilon}_i$ – effective strain rate, K – material consistency, m – coefficient equal 1 for Newtonian fluids and 0 for rigid–plastic materials, which obey Huber-Mises yield criterion ($\sigma_p = \sqrt{3}K$) and Levy-Mises flow rule. For typical metal forming processes the values of m are in the range [0,1] and relation between consistency and flow stress is:

$$K = \frac{\sigma_p}{\left(\sqrt{3}\right)^{m+1}\dot{\varepsilon}_i^m} \tag{2}$$

The mechanical model is coupled with the finite element solution of the Fourier heat transport equation:

$$\nabla \cdot k\nabla T + Q = \rho c_p \frac{\partial T}{\partial t} \tag{3}$$

where: k – heat conductivity, T – temperature, Q – rate of heat generation due to plastic work or due to transformation, ρ – density, c_p – specific heat, t – time.

3.2. Rheological model

Rheological models for hot forming and cold forming were developed. Coefficients in these models were determined using plastometric tests performed on the Gleeble 3800 simulator. The stress-strain curves obtained in the uniaxial compressing tests were processed by means of the inverse technique to eliminate the effect of friction and adiabatic heating. The inverse algorithm described by Szeliga et al. (2006) was used. It was found out after preliminary processing that the rheological model developed at the University of Sheffield (Davenport et al., 1999) and described also by Kowalski et al. (2000), was successfully fitted with the experimental stress-strain curves for hot forming of the investigated steel:

$$\sigma_p = \sigma_0 + (\sigma_{sse} - \sigma_0)\left[1 - \exp\left(-\frac{\varepsilon}{\varepsilon_r}\right)\right]^{\frac{1}{2}} - \begin{cases} 0 & \varepsilon \le \varepsilon_c \\ (\sigma_{sse} - \sigma_{ss})X_{dyn} & \varepsilon > \varepsilon_c \end{cases} \tag{4}$$

where:

$$\sigma_0 = \frac{1}{\alpha_0}\sinh^{-1}\left(\frac{Z}{A_0}\right)^{\frac{1}{n_0}};$$

$$\sigma_{ss} = \frac{1}{\alpha_{ss}}\sinh^{-1}\left(\frac{Z}{A_{ss}}\right)^{\frac{1}{n_{ss}}};$$

$$\sigma_{sse} = \frac{1}{\alpha_{sse}}\sinh^{-1}\left(\frac{Z}{A_{sse}}\right)^{\frac{1}{n_{sse}}};$$

$$\varepsilon_r = \frac{1}{3.23}\left[q_1 + q_2(\sigma_{ss(e)})^2\right];$$

$$Z = \dot{\varepsilon}\exp\left(\frac{Q_{def}}{R\widehat{T}}\right)$$

where: Z – Zener-Hollomon parameter, ε – strain, $\dot{\varepsilon}$ – strain rate, $\widehat{T}$ – absolute temperature, Q_{def} = 323900 J/mol – activation energy for deformation.

The model coefficients obtained by conducting the inverse analysis are given in table 2. It is noteworthy, that the model accounts for the effect of austenite grain size on the stress-strain curves trough the incorporation into it the dynamic recrystallization kinetics.

Table 2. *Coefficients in equation (4) for the steel with chemical composition given in table 1, obtained by optimization using inverse analysis.*

α_0	A_0	n_0	α_{ss}	A_{ss}	n_{ss}	α_{sse}	A_{sse}	q_1	q_2
0.02	1.26×10^{14}	19.31	0.00649	3.59×10^{13}	6.20	0.00649	1.91×10^{12}	0.63	3.64×10^{-11}

The rheological model for cold forming was developed, as well. To account for the deformation heating, compression tests were performed in the temperature range 20°C-300°C. Equation proposed by Hansel and Spittel (1979) was used to describe the flow stress of the investigated steel:

$$\sigma_p = A\varepsilon^m \exp(q\varepsilon)\dot{\varepsilon}^n \exp(\beta T) \tag{5}$$

where: T – temperature in °C, A, m, n, q, β - coefficients, which are determined using the inverse method (Szeliga et al., 2006).

Values of the coefficients obtained from the inverse analysis for the samples B1 and B2 are given in table 3. The final value of the cost function Φ, which is the square root erron between measured and calculated forces (Szeliga et al., 2006) and which represents accuracy of the inverse analysis, is given in the last column of this table. Selected flow stress curves are shown in figure 14. In is seen that influence of the temperature in the investigated range is negligible. Analysis of all results shows that the effect of the strain rate is small, as well.

Table 3. *Coefficients in equation (5) for the steel with chemical composition given in table 1, obtained by optimization using inverse analysis.*

sample	A	m	q	n	β	Φ
B1	1089.7	0.072	0.107	0.00464	0.0826	0.0299
B2	1033.6	0.0874	0.115	0.00509	0.0547	0.035

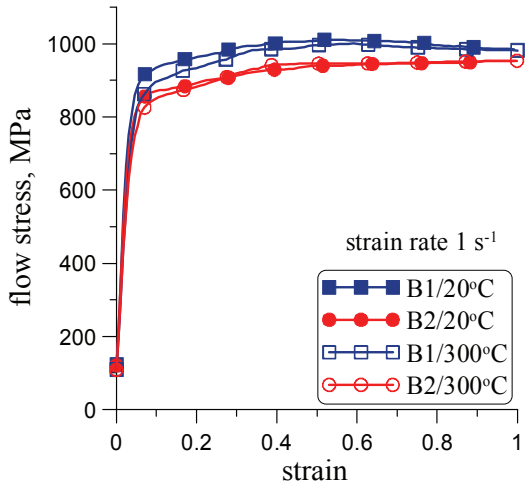

Fig. 14. Flow stress of the investigated bainitic steel obtained from the inverse analysis.

3.3. Microstructure evolution model

Development of the microstructure evolution model for the experimental bainitic steels, capable of predicting changes in the austenite microstructure occurring in the rod or wire rolling process, was one of the aims of the paper. The model equations allow the prediction of the following parameters and phenomena occurring in the deformed material:

- kinetics of the dynamic, metadynamic and static recrystallization,
- recrystallized grain size,
- kinetics of grain growth after recrystallization,
- static recovery.

A closed form equations are used to characterize the effect of initial austenite grain size, strain, strain rate, temperature and time on the microstructural evolution during and after deformation. This approach was widely adopted for microstructure modelling after pioneering works by Sellars and coworkers (Sellars, 1979; Sellars & McTeggart, 1972; Sellars & Whiteman, 1979) and has successfully been used in the modelling of hot rolling processes (eg. Pietrzyk, 1990; Głowacki et al., 1992; Pietrzyk et al., 1993; Pietrzyk et al., 1995; Buchmayr et al., 1993; Grossterlinden et al., 1994; Donnay et al., 1996; Kuziak, 1996; Majta et al., 1996; Lenard et al., 1999).

The stress relaxation experiments (Karjalainen et al., 1996) performed on the Gleeble 3800 simulator for the steel with the chemical composition given in table 1 were used to determine the coefficients in the models. The following equations were derived for the strain for recrystallization initiation (ε_c), strain to the peak occurrence in the flow curve (ε_p), strain to the onset of stable flow (ε_s), volume fraction of the dynamically recrystallized material (X_{DRX}), and the recrystallized grain size (D_{DRX}):

$$\varepsilon_c = 0.8\varepsilon_p \tag{6}$$

$$\varepsilon_p = 6.38\times10^{-4} D_0^{0.49} Z^{0.17} \tag{7}$$

$$\varepsilon_s = 5.25\times10^{-4} D_0^{0.5} Z^{0.2} \tag{8}$$

$$X_{DRX} = 1-\exp\left[-2.98\left(\frac{\varepsilon-\varepsilon_c}{\varepsilon_s-\varepsilon_c}\right)^2\right] \tag{9}$$

$$D_{DRX} = 923\, Z^{-0.11} \tag{10}$$

where: D_0 – initial austenite grain size, ε – strain, Z – Zenner–Hollomon parameter.

The dynamic recrystallization is followed by the metadynamic one in the time interval preceding the next deformation. The kinetics of the metadynamic recrystallization in Ti–steel are given by the following equation:

$$X_{MDRX} = 1-\exp\left[-0.693\left(\frac{t}{t_{0.5M}}\right)^{1.2}\right] \tag{11}$$

The time to 50% of metadynamic recrystallization is given by the equation:

$$t_{0.5M} = \left(1.47\times10^{-5}\right)\dot{\varepsilon}^{-0.8}\exp\left(\frac{120000}{R\widehat{T}}\right) \tag{12}$$

The metadynamically recrystallized grain size is larger by some 20% in comparison to dynamically recrystallized grain size developed during the deformation:

$$D_{DRX} = 1100\; Z^{-0.11} \tag{13}$$

Finally, the grain growth kinetics after metadynamic recrystallization is given by equation:

$$D(t)^{6.9} = D_{MRX}^{6.9} + 8.43\times10^{20}\exp\left(\frac{-323900}{R\widehat{T}}\right)t \tag{14}$$

The static recrystallization model is composed of 3 equations standing for the Avrami–type representation of the recrystallization kinetics, time to 50% recrystallization to proceed in deformed volume and recrystallized grain size:

$$X = 1-\exp\left[-0.693\left(\frac{t}{t_{0.5}}\right)^{1.7}\right] \tag{15}$$

$$t_{0.5} = 1.0\times10^{-13} D_0 \varepsilon^{-1.03} \dot{\varepsilon}^{-0.31} \exp\left(\frac{289488}{R\widehat{T}}\right) \quad (16)$$

$$D_{RX} = 17.624\varepsilon^{-0.38} \dot{\varepsilon}^{-0.05} D_0^{1.20} \exp\left(-\frac{44355}{R\widehat{T}}\right) \quad (17)$$

The following kinetics model for the grain growth after static recrystallization was developed by fitting the theoretical equation with the experimental results:

$$D(t)^5 = D_{RX}^5 + 2\times10^{20} \exp\left(\frac{-353562}{R\widehat{T}}\right) t \quad (18)$$

It is noteworthy that the grain growth kinetics is very sluggish in the experimental steel which can be accounted for by the dynamic precipitation of grain boundaries pinning particles of TiC precipitates.

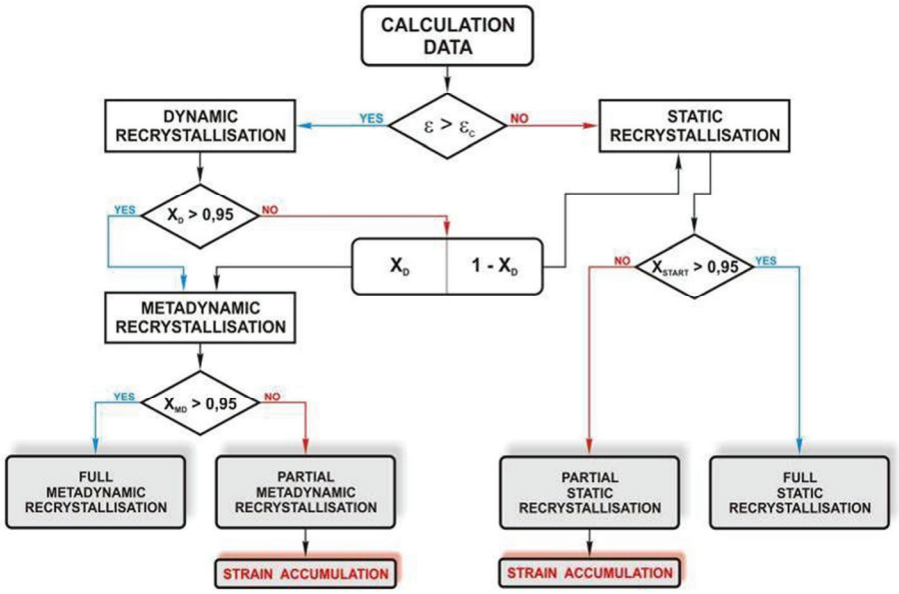

Fig. 15. *Structure of the austenite microstructure evolution model used for the simulation of bar and wire rod rolling processes.*

A general scheme of the numerical algorithm for the austenite microstructure evolution simulation during the rolling process is shown in figure 15.

3.4. Phase transformation model

A number of phase transformation models are available in the literature, from the simplest ones based on the Avrami equation (Avrami, 1939) to more advanced models based on phase field (Simmons et al., 2000) or solution of differential equation (Suehiro et al., 1992). Since the objective of the present work is prediction of transformation temperatures and volume fractions of structural components, a simple model based on Avrami equation is selected:

$$X = 1 - \exp\left(-kt^n\right) \quad (19)$$

where: X – transformed volume fraction, k, n – coefficients.

Theoretical considerations show that, according to the type of transformation (nucleation and growth process, site saturation process) a constant value of coefficient n in equation (19) can be used. On contrary, value of the coefficient k must vary with temperature in a way linked to the form of a TTT diagram. The formalism of the function $k = f(T)$ must be carefully chosen to describe properly the temperature dependence of k. Various functions were tested in the present work. A modified Gaussian function proposed by Donnay et al. (1996) was selected for the ferritic transformation:

$$k = k_{\max} \exp\left[-\left(\frac{T - T_{nose}}{a_8}\right)^{a_7}\right] \quad (20)$$

The four coefficient k_{max}, T_{nose}, a_7, a_8 allow description of all shapes of the TTT curves in a quite intuitive way. Thus, k_{max} is the maximum value of k, T_{nose} is a temperature position of the nose of the Gaussian function, a_7 is proportional to the nose width thickness at mid height and a_8 is related to the sharpness of the curve. The equations, which are used to calculate coefficients k_{max} and T_{nose} are:

$$k_{\max} = \frac{a_5}{D_\gamma} \quad (21)$$

$$T_{nose} = Ae_3 + \frac{400}{D_\gamma} - a_6 \quad (22)$$

where: D_γ – austenite grain size at the beginning of transformation.

Slightly simpler function was selected for the pearlitic transformation:

$$k = \frac{a_{14}}{D_\gamma^{a_{16}}} \exp\left(a_{13} - a_{12}T\right) \tag{23}$$

In the bainitic transformation relation on the grain size D_γ is neglected:

$$k = a_{23} \exp\left(a_{22} - a_{21}T\right) \tag{24}$$

Function (19) does not require the incubation time. It is assumed that ferritic transformation begins when the volume fraction of ferrite achieves 5%. Incubation times for the remaining transformations (τ_p, τ_b) are calculated as:

$$\tau_P = \frac{a_9}{\left(\mathrm{Ae}_1 - T\right)^{a_{11}}} \exp\left(\frac{a_{10} \times 10^3}{R\widehat{T}}\right) \quad \text{pearlitic} \tag{25}$$

$$\tau_b = \frac{a_{17}}{\left(T_b - T\right)^{a_{19}}} \exp\left(\frac{a_{18} \times 10^3}{R\widehat{T}}\right) \quad \text{bainitic} \tag{26}$$

Additional relationships in the model are given in table 4. Equilibrium concentrations $c_{\gamma\alpha}$ and $c_{\gamma\beta}$ in table 4 are calculated as functions of temperature. Coefficients in these functions were determine for the considered chemical compositions of steel (table 1) using ThermoCalc software and they are given in table 5.

Table 4. *Additional equations in the model.*

$c_\gamma = \dfrac{\left(c_0 - X_f c_\alpha\right)}{1 - X_f}$	$X_{f0} = \dfrac{c_{\gamma\alpha} - c_0}{c_{\gamma\alpha} - c_\alpha}$
$c_\alpha = -0.069 + 0.000435T - 9.1658\times10^{-7}T^2 + 6.487\times10^{-10}T^3$ for $T < 637^\circ$C $c_\alpha = -0.0487268 + 0.00017839T - 1.50788\times10^{-7}T^2$ for $T > 637^\circ$C	
$c_{\gamma\alpha} = c_{\gamma\alpha0} + c_{\gamma\alpha1}T$	$c_{\gamma\beta} = c_{\gamma\beta0} + c_{\gamma\beta1}T$

Notation: c_γ – average carbon content in austenite, c_α – carbon content in ferrite, c_0 – carbon content in steel, $c_{\gamma\alpha}$ – carbon concentration in austenite at the γ-α boundary, $c_{\gamma\beta}$ – carbon concentration in austenite at the γ-cementite boundary.

Table 5. *Parameters in equations describing equilibrium carbon contents in table 4.*

$c_{\gamma\alpha0}$	$c_{\gamma\alpha1}$	$c_{\gamma\beta0}$	$c_{\gamma\beta1}$
4.8365	-0.005818	-1.09	0.00259

Simulation of phase transformations starts with equation (18) when the temperature drops below Ae_3. The transformed volume fraction X_f is calculated with respect to the maximum volume fraction of ferrite X_{f0} in the current temperature. Thus, this volume fraction of ferrite with respect to the whole volume of the body is $F_f = X_{f0}X_f$. During numerical simulation in the varying temperature the current value of X_f calculated from equation (18) has to be corrected to account for the change of the equilibrium (maximum) volume of ferrite X_{f0}, which according to equation in table 2 is a function of temperature:

$$X_f^{i+1} = X_f^i \frac{X_{f0}\left(T^i\right)}{X_{f0}\left(T^{i+1}\right)} \tag{27}$$

where: i – iteration number.

Simulation continues until the transformed volume achieves 1. However, when carbon content in austenite achieves the limiting value $c_{\gamma\beta}$ (see Table 2), the austenite-pearlite transformation begins in the remaining volume of austenite.

Bainite start temperature (T_b) and martensite start temperature (T_m) are functions of the chemical composition of the austenite:

$$T_b = a_{20} - 425[\mathrm{C}] - 42.5[\mathrm{Mn}] - 31.5[\mathrm{Ni}] - 70[\mathrm{Cr}] \tag{28}$$

$$T_m = a_{26} - a_{27}c_\gamma \tag{29}$$

Fraction of austenite, which transforms into martensite is calculated according to the model of Koistinen and Marburger, described also in (Umemoto et al., 1992; Pietrzyk et al., 2003):

$$X_m = 1 - \exp\left[-0.011\left(T_m - T\right)\right] \tag{30}$$

Equation (30) represents volume fraction of martensite with respect to the whole volume of austenite, which was remaining at the temperature T_M. The volume fraction of martensite with respect to the whole volume of the material is:

$$F_m = \left(1 - F_f - F_p - F_b\right)\left\{1 - \exp\left[-0.011\left(T_m - T\right)\right]\right\} \tag{31}$$

where: F_f, F_p, F_b – volume fractions of ferrite, pearlite and bainite with respect to the whole volume of the sample.

Additivity rule (Scheil, 1935) is applied in the model to account for the temperature changes during transformations.

Identification of the phase transformation model was performed next. As it has been mentioned, coefficients in equations describing equilibrium concentrations of carbon in table 4 were determined using ThermoCalc software and they are given in table 5. Coefficients $\mathbf{a} = \{a_1 \ldots a_{27}\}$ in the phase transformation model were determined using inverse analysis of the dilatometric tests for the investigated steel. Basic principles of the inverse method are described in a number of publications, see for example (Szeliga et al., 2006). The most frequent applications of the inverse method in metallurgy are connected with determination of coefficients in rheological models of materials subjected to plastic deformation. This solution, which is used in section 3.2 of the present paper, is well described in the literature (Szeliga et al., 2006; Forestier et al., 2002).

Applications of the inverse approach to the identification of the phase transformation model are less frequent. The algorithm used in the present work is based on (Kondek et al., 2003) and the general idea of this algorithm is described briefly below. Mathematical model of an arbitrary phase transformation can be described by a set of equations:

$$\mathbf{d} = F(\mathbf{a}, \mathbf{p}) \tag{32}$$

where: $\mathbf{d} = \{d_1,..,d_r\}$ - vector of start and finish temperatures of transformations and volume fractions of structural components in the room temperature, which are measured in the dilatometric tests performed with constant cooling rates, $\mathbf{a} = \{a_1,..,a_l\}$ - vector of coefficients of the model, $\mathbf{p} = (p_1,..,p_k\}$ - vector of such process parameters as cooling rates, austenite grain size and deformation of austenite.

When vectors **p** and **a** are known, the solution of the problem (32) is called a direct solution. Inverse solution of the task (32) is defined as determination of the components of the vector **x** for known vectors **d** and **p**. When the problem is liner, the inverse function can be found and the problem can be often solved analytically. For phase transformations these relations are strongly nonlinear and optimization techniques are used to solve the inverse task.

The objective of the inverse analysis is determination of the optimum components of the vector **a.** It is achieved by searching for the minimum, with respect to the vector **a**, of the objective function defined as a square root error between measured and calculated components of the vector **d**:

$$\Phi(\mathbf{a}, \mathbf{p}) = \sum_{i=1}^{n} \beta_i [\mathbf{d}_i^c(\mathbf{a}, \mathbf{p}_i) - \mathbf{d}_i^m]^2 \tag{33}$$

where: $\mathbf{d}_i^m$ – vector containing measured values of output parameters, $\mathbf{d}_i^c$ – vector containing calculated values of output parameters, β_i – weights of the points, ($i = 1 .. n$), n – number of measurements.

Measurements $\mathbf{d}_i^m$ are obtained from the dilatometric tests carried out with constant cooling rates. Components $\mathbf{d}_i^c$ are calculated using one of the models of the direct problem, which are described above.

Identification of parameters of the phase transformation model is composed of two parts. The first is solution of the direct problem, based on the model. The second part is solution of the inverse problem, in which optimization techniques are used.

Results of dilatometric tests (see section 3.2), including measurements of the start and end temperatures for transformation and volume fractions of phases after cooling to room temperature, are used as an input to the inverse analysis. Thus, in the particular case of phase transformations the objective function (33) is defined as:

$$\Phi(\mathbf{a}, \mathbf{p}) = \sqrt{\frac{1}{n}\sum_{i=1}^{n}\left(\frac{T_{im} - T_{ic}}{T_{im}}\right)^2 + \frac{1}{k}\sum_{i=1}^{k}\left(\frac{X_{im} - X_{ic}}{X_{im}}\right)^2} \tag{34}$$

where: T_{im}, T_{ic} – measured and calculated start and end temperatures of phase transformations, n – number of temperature measurements, X_{im}, X_{ic} – measured and calculated volume fractions of phases at room temperature, k – number of measurements of volume fractions of phases.

The values of the coefficients **a** obtained from the inverse analysis are given in table 6 for the deformation temperature of 1050°C and in table 7 for the deformation temperature of 870°C. In general, the whole model for all transformations may contain all together 27 coefficients (Kondek et al., 2003). However, only 23 of them are active in the transformation model for the considered bainitic steel and are used in the present work. Model with the coefficients in table 6 was validated. It was used to simulate all the dilatometric tests, which were performed

Table 6. *Coefficients in the phase transformation model calculated using inverse analysis for the deformation temperature of 1050°C.*

a_4	a_5	a_6	a_7	a_8	a_9	a_{10}	a_{11}	a_{12}	a_{13}	a_{14}	a_{15}
1.685	0.016	224.1	45.08	1.174	7.35	0.	0.	1.87	0.088	6.29	0.2133
a_{16}	a_{17}	a_{18}	a_{19}	a_{20}	a_{21}	a_{22}	a_{23}	a_{24}	a_{26}	a_{27}	
0.48	1.289	0.175	0.	714.6	1.713	4.04	0.187	1.453	452	63.94	

Table 7. *Coefficients in the phase transformation model calculated using inverse analysis for the deformation temperature of 870°C.*

a_4	a_5	a_6	a_7	a_8	a_9	a_{10}	a_{11}	a_{12}	a_{13}	a_{14}	a_{15}
2.486	0.611	205.7	74.72	2.894	12.28	10.6	0.0694	1.87	0.0879	6.291	2.133
a_{16}	a_{17}	a_{18}	a_{19}	a_{20}	a_{21}	a_{22}	a_{23}	a_{24}	a_{26}	a_{27}	
0.48	2.297	0.863	0.0823	705.6	1.713	4.039	0.187	1.453	437	3.28	

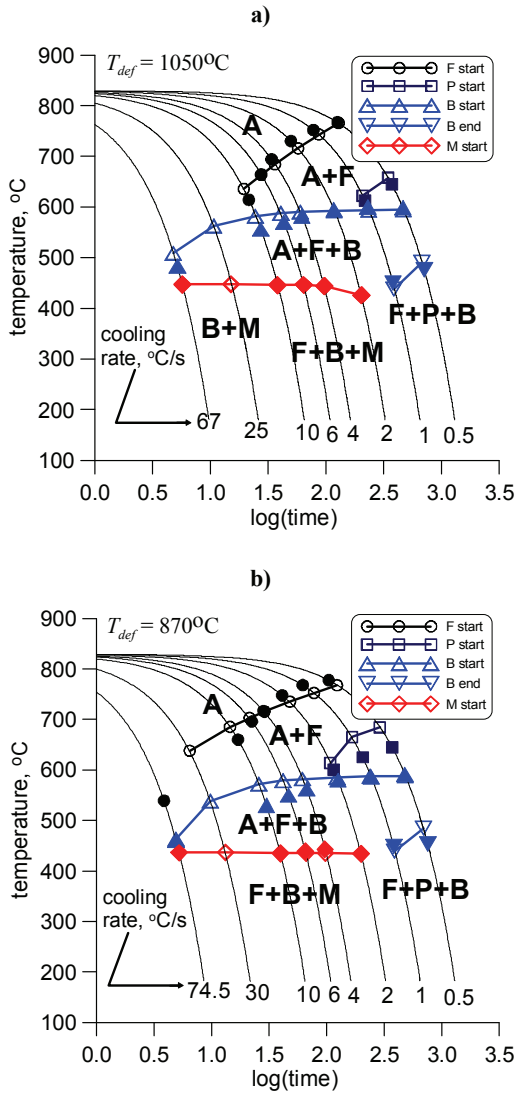

Fig. 16. *Comparison of the predictions of the optimized phase transformation model (coefficients in tables 6 and 7) with measurements for the transformations start and end temperatures, deformation temperature of 1050°C (a) and 870°C (b).*

and are described in section 2.3 of this paper. Figure 16 shows comparison of the measured (filled symbols) and predicted (open symbols) start and end temperatures for the phase transformations. Shape of the symbol refers to the temperature in the legend. Analysis of the results shows that the model predicts quite well start and end temperatures for transformations, although the accuracy is slightly worse for the non recrystallized austenite.

Phase transformation model with the optimized coefficients was implemented in the FE code and used in simulations of the accelerated cooling after hot rolling.

4. SIMULATION OF THE MANUFACTURING CHAIN

Schematic illustration of the manufacturing chain for fasteners, which was investigated in the present work, is shown in figure 17. This manufacturing chain was simulated using models described in Chapter 3 of this paper. Various types and dimensions of fasteners were considered but the analysis in the present paper is constrained to the standard screw M8×25 according to ISO 4017. Selected results of simulations are presented below.

4.1. Hot rolling of rods

Hot rolling of rods or wires is the first link in the manufacturing chain, which is considered. This process is well researched. The objective of simulations is prediction of microstructure evolution during rolling. The models described in sections 3.1 (FE model), 3.2 (rheological model) and 3.3 (microstructure

evolution model), were applied. Wires of 8 mm diameter are now used for manufacturing M8 screw and rolling of these wires are simulated below. For comparison, rods with the diameter of φ15.8 mm are analysed, as well.

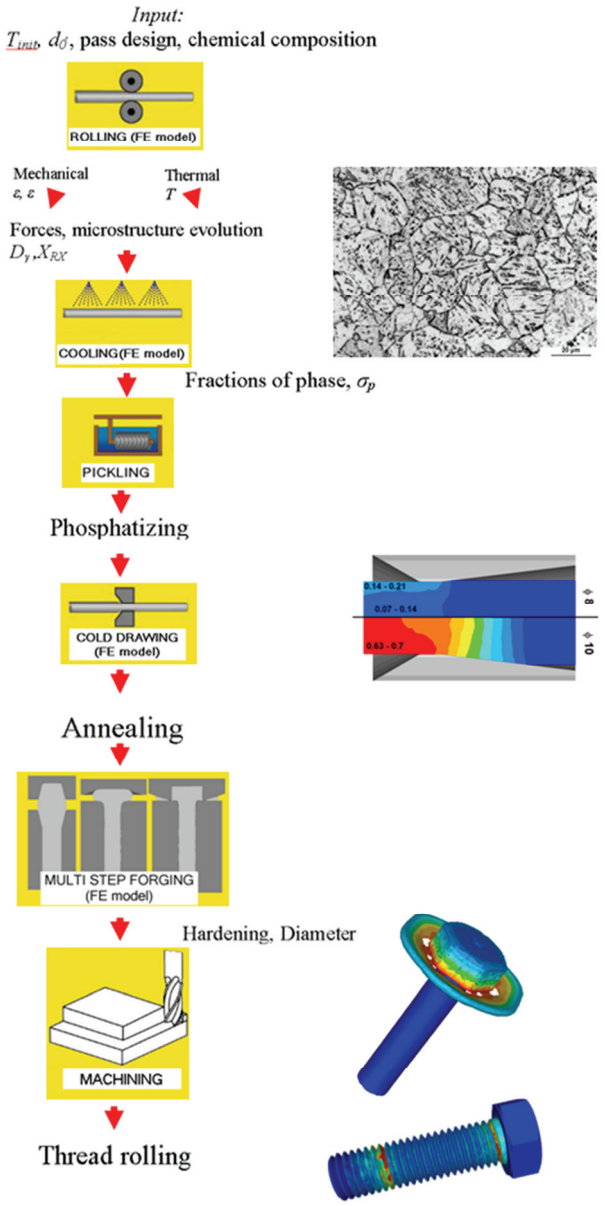

Fig. 17. *Schematic illustration of the manufacturing chain for fasteners.*

The rolling process for bainitic steel rods was conducted on the three–high laboratory rolling mill. For rod rolling trials, the square bars having 49×49 mm in cross section were prepared from experimental ingots by means of hot pressing. The bars were subject to the pre–rolling in 3 oval-round-square passes to the square having 23×23 mm in cross section, followed by 4 oval-round passes during the finish rolling to the bar having diameter of φ15.8 mm. The finish rolling temperature was varied by changing the holding time prior to the first pass. After rolling, the bars were subjected to the accelerated cooling with pressurized air. The cooling rates at the cooling device were varied by applying different air pressure.

The thermal–mechanical and microstructure evolution models were used to simulate microstructure of bars and wire rods. The most important module of the numerical calculation include the austenite grain size evolution predictor. The evolution model describes austenite grain size as a function of initial grain size, strain, strain rate, temperature and time, see section 3.3. The algorithm of figure 15 was implemented in the FE Forge commercial code. The results of calculations of the austenite grain size during the φ15.8 mm diameter rod rolling process are shown in figure 18 for two finish rolling temperatures, 1050 and 950°C. The sketches in these figures pertain to the distribution of austenite grain size after seven seconds of cooling after the last pass. Due to the symmetry, only one quarter of the bar is shown in these figures.

The results of the simulations compare well with the metallographic measurements conducted on bars cooled at rate of 3.2°C/s in areas indicated in figure 19. In the bars, prior austenite grain boundaries encompass the bainitic ferrite domains, and thus, are clearly distinguished in the microstructure (figure 20). The results of the grain size measurements are given in table 8. These results show that a relatively uniform grain size was achieved in the bars, and that the increase in the last deformation temperature from 1050 to 950°C had significant effect on the austenite microstructure evolution.

Table 8. *Results of the austenite grain size measurements in the areas A, B, C of the bars.*

T_{fr}, °C	Grain size, μm		
	A	B	C
1050	39.7	32.5	35.5
950	28.3	27.3	29.8

The rolling process for bainitic steel wires was conducted on the pilot rolling mill in the TU-BA Freiberg. The parameters of this mill are described by Hadasik et al. (2006). For wire rolling trials, the square bars having 44×44 mm in cross section were prepared from experimental ingots by means of hot pressing. The bars were subjected to rough rolling from the initial geometry to a wire of φ12 mm in diameter. The rolling was performed in 12 passes. After the rough rolling, the finish rolling was performed continuously in four steps to a diameter of

φ8 mm. The work-piece temperature before the first pass was 870°C, and before the last pass was 900°C. The increase in the temperature is connected with heat generated by plastic deformation. The finishing rolling speed was 20 m/s. Similarly to rod rolling, simulations of this process were performed and microstructure was analysed.

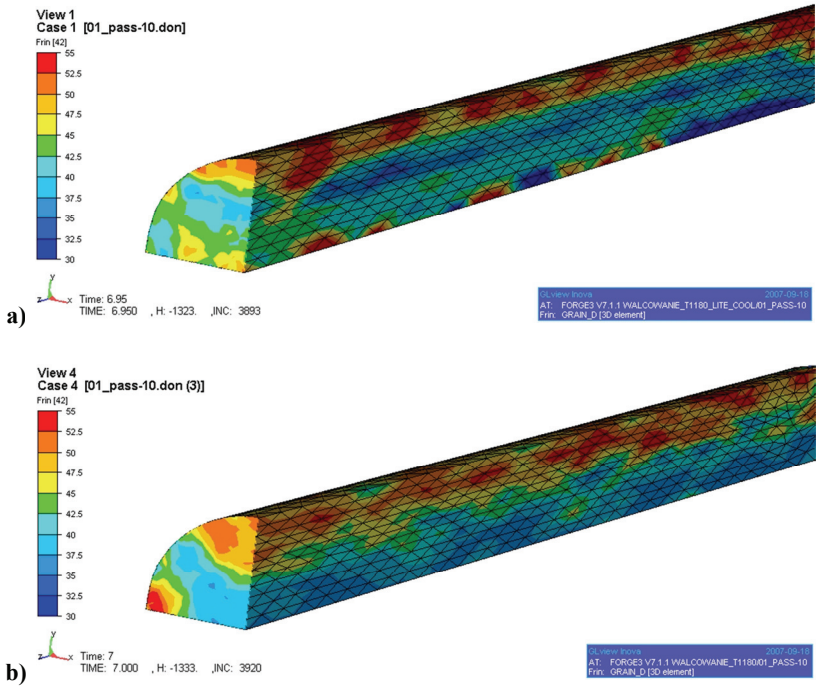

Fig. 18. *Grain size distribution in the bar after seven seconds of cooling at a rate 3°C/s following the last pass with finish rolling temperature 1050°C (a) and cooling at a rate 3.2°C/s following the last pass with finish rolling temperature 950°C (b).*

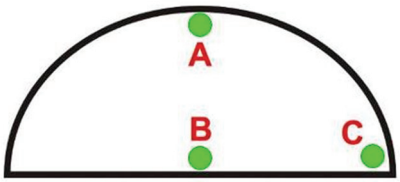

Fig. 19. *Locations at the bar cross section where the measurement of the austenite grain size was conducted.*

Analysis of all results of simulations shows that some discrepancies between the results of simulation and measurement of the austenite grain size occurs. These discrepancies can be connected to the fact that the boundary conditions in the rolling experiments were identified based upon the surface measurement of temperature with pyrometer. Results of simulations of grain size during hot rolling were used as input data for further simulation of phase transformations during accelerated cooling of rods and wires.

4.2. Accelerated cooling

After hot rolling the rods and the wires were cooled using air under pressure. Accelerated cooling was simulated using FE software. The phase transformation model described in section 3.3 was implemented in the FE code following the idea described by Pietrzyk & Kuziak (1999). The heat transfer coefficient of 170 W/m^{2}K was assumed. Temperature changes and kinetics of transformations at the centre of the rod and the wire are shown in figure 21a. Solid lines and filled symbols represent results for the rod and dotted lines and open symbols represent results for the wire. It is seen in figure 21a that cooling of the wire is faster and, in consequence, the volume fraction of the bainite is larger. Figure 21b shows distribution of the volume fractions of the structural components along the radius of the rods and wires. It is seen that this distribution is reasonably uniform.

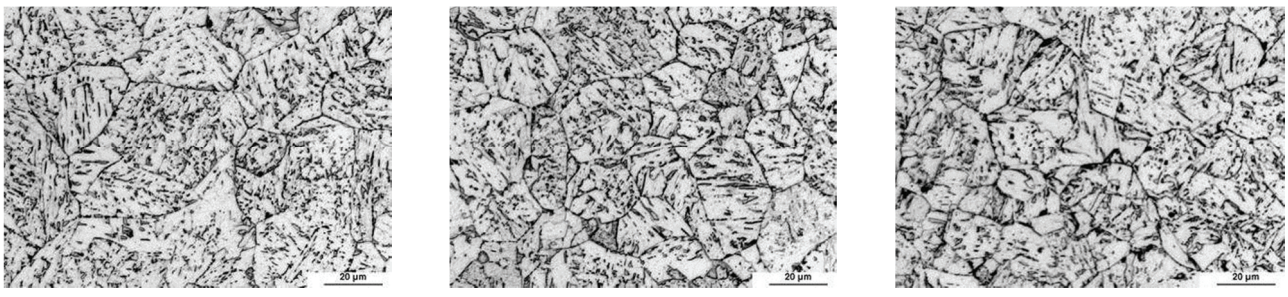

A **B** **C**

Fig. 20. *Microstructure in the locations A, B, C of the bar rolled with last deformation temperature around 950°C.*

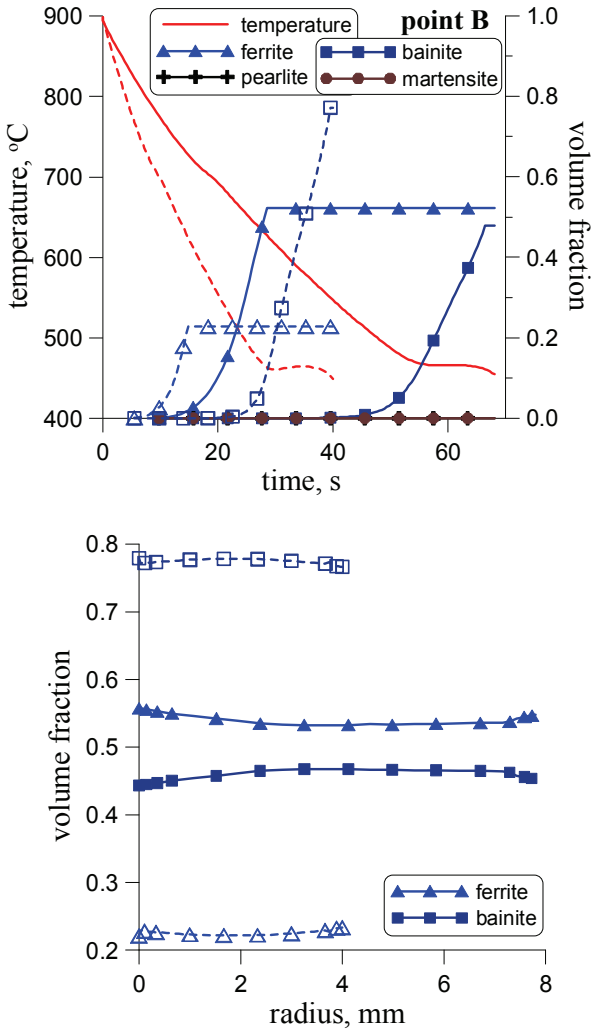

Fig. 21. *Temperatures and kinetics of transformations at the centre of the rod and the wire (a) and distribution of volume fractions along the radius of the rod and the wire (b).*

Hot rolled rods or wires are used as stock material for cold forming. Rheological model for this material has been developed, see section 3.2 and it was used in simulations of cold drawing and forging.

4.3. Drawing

Drawing process is an important link in the manufacturing chain for fasteners. Reduction of the rod diameter, improvement of the rod dimensional accuracy and hardening of the material are the main objectives of the drawing process. Determination of strains and stresses in drawing of the investigated bainitic steel was the goal of simulations.

Before drawing the bainitic steel wires are subjected to pickling and preparing of the surface by cascade pickling in HCL, cascade water deep rinsing at 28°C, activation SALE TZ, phosphatizing at 55°C for 9 min, cascade water deep rinsing at 28°C, neutralization at 40°C and hot air drying at 120°C. These are standard operations and are not considered in the present work. More information on surface preparing can be found in (Kuziak et al., 2011a). The drawing process was carried out on single-hole drawing machine with the speed of 1 m/s, with usage of sintered carbide drawing die and lubricant TRXIT CV. Drawing parameters were: die semi angle 8°, length of the calibrating part of the die 2-3 mm, friction coefficient 0.03 (Madej et al., 2009b). The objective of simulations was to evaluate possibility of increasing the diameter of wires. Thus, the initial diameters D_0 = 8 and 10 mm were considered. The final diameter was D_1 = 7.7 mm, which is the size of the stock material for manufacturing the screw M8.

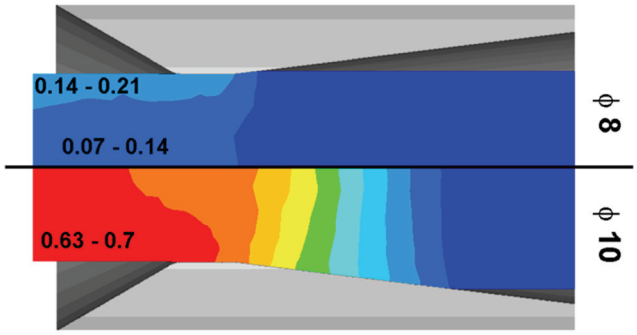

Fig. 22. *Comparison of the strain distribution during drawing for the input diameters 8 mm and 10 mm.*

Strain distribution during drawing is shown in figure 22. As expected, higher strains are accumulated in the wire rod with D_0 = 10 mm (0.63-0.7 at the surface, comparing to 0.14-0.21 for D_0 = 8 mm), what eventually leads to higher hardness. That is especially important in the surface area, where the bolt thread is rolled during the last stage of the manufacturing stage. The increase of the input diameter for drawing has to be preceded by the analysis of the die wear. This analysis is combined with the forging process and is presented in section 4.5.

4.4. Multi step forging

The standard screw M8×25 according to ISO 4017 grade 8.8 according to ISO 898 part 1, as presented in (Kuziak et al., 2011a), was selected as an example of the analysis. The annealing process was performed before forging. The annealing was carried out on bell annealing furnace EBNER including following stages: heating to 730°C, holding for 3h, slow cooling (10°C/h) to 680°C and maintaining for 5h. The cold forging process was carried out on the multi stage press TDZR 8.

Calculated distributions of strains at the cross sections of this screw during forging are shown in figure 23. The level of strains allows obtaining the required hardness of the screw, in particular in the head area, without heat treating according to standard procedure.

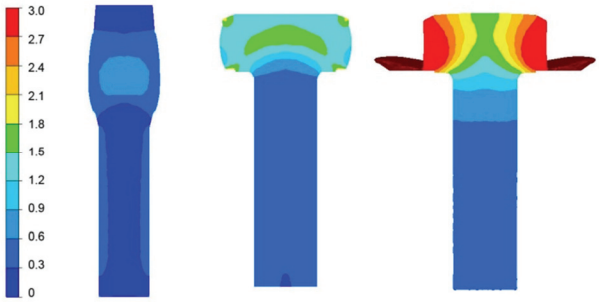

Fig. 23. *Strain distribution during forging of the screw.*

Machining and rolling of the thread were the last two links in the manufacturing chain. These operations were simulated (see results in figure 24) but there were no modification introduced in these operations.

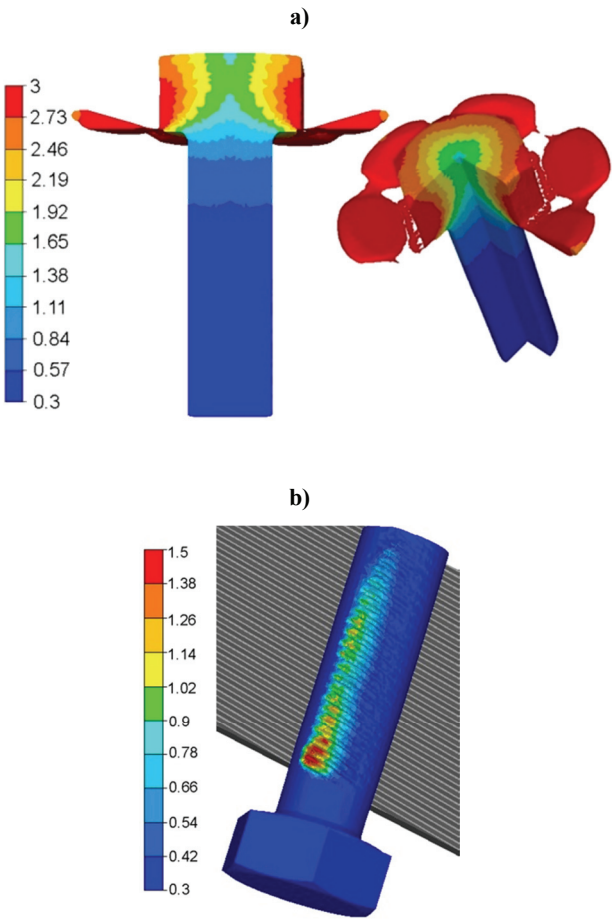

Fig. 24. *Results of simulations of machining (a) and rolling of the thread (b) - distributions of strains are presented.*

4.5. Die wear

It is expected that larger strains for the input drawing diameter φ10 mm will involve increase of the tool wear. Therefore, analysis of the die wear was performed. Volume of wear due to sliding was calculated according to Archard (1953) model. The results for drawing are shown in figure 25. Tool wear during the two stages of forging is presented in figure 26, see also (Madej et al., 2009a).

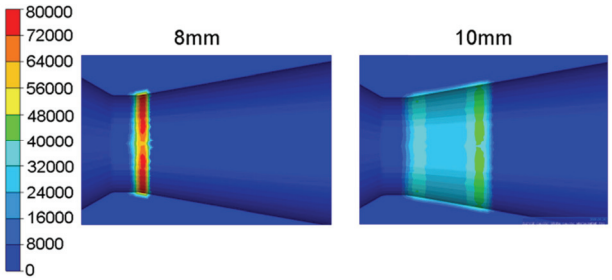

Fig. 25. *Die wear during drawing of ϕ8 mm (left) and ϕ10 mm (right) rods.*

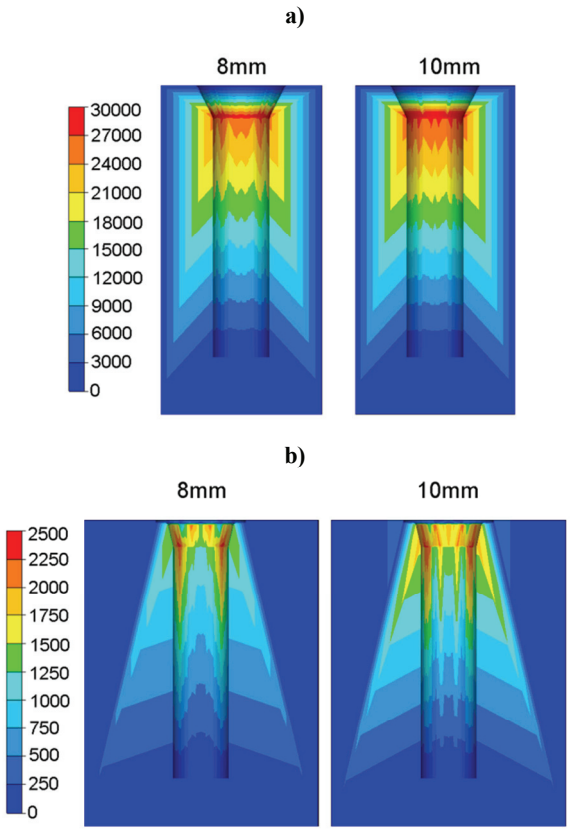

Fig. 26. *Die wear during the second (a) and third (b) stage of forging after drawing of ϕ8 mm and ϕ10 mm rods.*

Large wear of drawing die, due to localized strains, is observed in the variant I (D_0 = 8 mm). Value of the wear is large but it is very localized. As far as forging is considered, due to larger hardening variant II (D_0 = 10 mm) the die wear increases, in

particular in the second stage of the process. Due to low die wear, results for the first stage of forging are not shown.

Die wear during forging of bainitic steel screws was compared with that observed for DP steel and for the commonly used now carbon-manganese steel. Due to larger stresses, die wear for the bainitic steels is slightly larger. The problem of accurate evaluation of the die wear and optimization of the manufacturing costs requires more extensive investigation.

4.6. Industrial trials

On the basis of the performed simulations the following manufacturing chain parameters were proposed: hot rolling with the finishing temperature 980°C or 800°C, accelerated cooling (3-5°C/s), pickling, phosphatizing, cold drawing (reduction 7-10%), annealing, 3-step cold forging, machining and rolling of thread. In the hot forming the finishing rolling temperature and conditions of the accelerated cooling are the main parameters, which control the morphology and properties of bainitic steels. These parameters were investigated in the laboratory tests (section 2.3) and the best technology was proposed. Industrial trials were performed for the cold forming operations in the KOELNER Łańcucka Fabryka Śrub, see (Kuziak et al., 2011a) for more details. Bainitic steels in the states B1 and B2 were compared with the C-Mn steel, which is used now in the factory. After the press set-up the batches were made of all grades of steel without adjustments of tools. The dimensional parameters were compatible with ISO 4017. After forging process the tensile tests were performed according to DIN 898, in order to compare mechanical properties. The tensile stress values are given in table 9. It is seen that the highest properties were obtained for the bainitic steel B1 (finishing rolling temperature 980°C).

Table 9. *Strength of the investigated screws after forging.*

Property	C-Mn	B1	B2
R_m, MPa	860	1105	993
$R_{p0.2}$, MPa	680	866	825

5. DISCUSSION AND CONCLUSIONS

Numerical analysis of manufacturing chain for fasteners has shown that, as far as manufacturing of high strength parts is considered, bainitic steel can be a good substitution for the carbon-manganese steel, which is commonly used now, as well as for the DP steel, which has recently been often introduced to increase the strength of products. Proper screw geometry and mechanical properties were achieved for the bainitic steels without heat treatment. Relatively easy thermomechanical processing during hot rolling of these steels is their main advantage over the DP steels. This is an important economical aspect in favour. Another incentive of using bainitic steels for the production of fasteners is connected to the production of screws that are sensitive to heat treatment defects, such as cracks and decarburisation. Increased die wear is the factor detracting application of the bainitic steels.

The ferritic-bainitic steel having the specified mechanical properties can be obtained by varying its chemical composition, monitoring the parameters of its thermomechanical treatment during rolling and choosing the proper parameters for accelerated cooling. The hardness distribution in screws head can be effectively affected by changing the forging technology (pass design). As a result, bainitic steels can be applied to the production of screws with low cross section in the head area. This particularly concerns the screws produced according to ISO 4014, EN 1662, ISO 10642, DIN 6921, ISO 8676, ISO 8765 etc. In this case, plastic deformation introduces substantial inhomogeneity and, as a result, an increased susceptibility for cracks initiation during quenching.

On the basis of the performed simulations and industrial trials the following manufacturing chain parameters for bainitic steel fasteners are proposed: hot rolling with the finishing temperature 900-980°C, accelerated cooling (3-3.5°C/s, finished at 400-450°C), pickling, phosphatizing, cold drawing (reduction 7-10%), annealing, 3-step cold forging, machining and rolling of thread. It was observed that decreasing the finishing rolling temperature to 800°C or increasing the finishing temperature of accelerated cooling to 550°C lead to decrease of the product properties. Increase of the reduction in drawing results in an increase of the forging die wear.

ACKNOWLEDGEMENTS

Financial assistance of the MNiSzW, project no. R15 032 03, is acknowledged.

REFERENCES

Archard, J.F., 1953, Contact and rubbing of flat surfaces, *Journal of Applied Physics*, 24, 981-988.

Avrami, M., 1939, Kinetics of phase change I, *J. Chem. Phys*., 7, 1103–1112.

Bhadeshia, H.K.D.H., Edmonds, D.V., 1980, The mechanism of bainite formation in steels, *Acta Metallurgica*, 28, 1265-1273.

Buchmayr, B., Samoilov, A., Lachmann, L., Aigmuller, G., 1993, A fundamental TMCP rolling model for the prediction and optimisation of microstructure and properties of HSLA steels, *Proc. Conf. Modelling of Metal Rolling Processes*, London, 134-148.

Davenport, S.B., Silk, N.J., Sparks, C.N., Sellars, C.M., 1999, Development of constitutive equations for the modelling of hot rolling, *Materials Science and Technology*, 16, 1-8.

Donnay, B., Herman, J.C., Leroy, V., Lotter, U., Grossterlinden, R., Pircher, H., 1996, Microstructure evolution of C-Mn steels in the hot deformation process: the STRIPCAM model, *Proc. 2nd Conf. Modelling of Metal Rolling Processes*, eds. Beynon, J.H., Ingham, P., Teichert, H., Waterson, K., London, 23-35.

Forestier, R., Massoni, E., Chastel, Y., 2002, Estimation of constitutive parameters using an inverse method coupled to a 3D finite element software, *Journal of Materials Processing Technology*, 125, 594-601.

Glowacki, M., Kedzierski, Z., Kusiak, H., Madej, W., Pietrzyk, M., 1992, Simulation of metal flow, heat transfer and structure evolution during hot rolling in square-oval-square series, *Journal of Materials Processing Technology*, 34, 509-516.

Grossterlinden, R., Kawalla, R., Lotter, U., Pircher, H., 1994, FEM Calculations and Simulation of Evolution of Microstructure during the Hot Rolling of Flat Products - Part I and II, *Metallurgy and Foundry Engineering*, 20, 319-341.

Hadasik, E., Kuziak, R., Kawalla, R., Adamczyk, M., Pietrzyk, M., 2006, Rheological model for simulation of hot rolling of new generation steel strips for automotive industry, *steel research international*, 77, 927-933.

Hansel, A., Spittel, T., 1979, *Kraft- und Arbeitsbedarf Bildsamer Formgebungs-verfahren*, VEB Deutscher Verlag fur Grundstoffindustrie, Leipzig.

Hoff, N.J., 1954, Approximate Analysis of Structures in the Presence of Moderately Large Steps Deformation, *Quart., Appl. Mech*., 2, 49.

Karjalainen, L.P., Perttu, J., 1996, Characteristics of static and metadynamic recrystallization strain accumulation in hot deformed austenite as revealed by stress relaxation method, *ISIJ International*, 36, 729-736.

Koistinen, D.P., Marburger, R.E., 1959, A general equation prescribing the extent of the austenite-martensite transformation in pure iron-carbon alloys and plain carbon steels, *Acta Metallurgica*, 7, 59-60.

Kondek, T., Kuziak, R., Pietrzyk, M., 2003, Finite Element Modelling of Deformation of Steels in Two-Phase Range of Temperatures, *Proc. COMPLAS VII*, eds, Owen, D.R.J., Onate, E., Suarez, B., CIMNE, Barcelona, CD ROM.

Kowalski, B., Sellars, C.M., Pietrzyk, M., 2000, Development of a computer code for the interpretation of results of hot plane strain compression tests, *ISIJ International*, 40, 1230-1236.

Kuziak, R., Glowacki, M., Pietrzyk, M., 1996, Modelling of plastic flow, heat transfer and microstructure evolution during rolling of eutectoid steel rods, *Journal of Materials Processing Technology*, 60, 589-596.

Kuziak, R., Pidvysots'kyy, V., Drozdowski, K., 2009, Validation of the thermo-mechanical-microstructural model of hot forging process, *Computer Methods in Materials Science*, 9, 424-434.

Kuziak, R., Skóra, M., Węglarczyk, S., Paćko, M., Pietrzyk, M., 2011a, Computer aided design of the manufacturing chain for fasteners, *Computer Methods in Materials Science*, 11, 243-250.

Kuziak, R., Milenin, A., Paćko, M., Pietrzyk, M., 2011b, Fasteners of bainitic steels manufactured by drawing and forging, *Hutnik-Wiadomości-Hutnicze*, 78, 74-77.

Lenard, J.G., Pietrzyk, M., Cser, L., 1999, *Mathematical and physical simulation of the properties of hot rolled products*, Elsevier, Amsterdam.

Madej, Ł., Szeliga, D., Kuziak, R., Pietrzyk, M., 2007, Physical and numerical modelling of forging accounting for exploitation properties of products, *Computer Methods in Materials Science*, 7, 397-405.

Madej, Ł., Węglarczyk, S., Pietrzyk, M., 2009a, Influence of technological parameters of manufacturing chain for steel bolts on die wear, *Hutnik-Wiadomości Hutnicze*, 76, 620-622.

Madej, Ł., Węglarczyk, S., Pietrzyk, M., 2009b, Simulation of drawing as an important stage in the steel bolt manufacturing chain, *Hutnik-Wiadomości Hutnicze*, 76, 71-73.

Majta, J., Munther, P., Lenard, J.G., Kedzierski, Z., Pietrzyk, M., 1996, Finite-element technique applied to the simulation of thermal, mechanical and microstructural evolution during rolling of high Nb steel, *Proc. 5th ICTP*, Columbus, I, 19-22.

Norton, F.H., 1929, *Creep of steel at high temperature*, McGraw Hill, New York.

Pietrzyk, M., 1990, Finite element based model of structure development in the hot rolling process, *Steel research*, 61, 603-607.

Pietrzyk, M., Kędzierski, Z., Kusiak, H., Madej, W., Lenard, J.G., 1993, Evolution of the microstructure in the hot rolling process, *Steel Research*, 64, 549-556.

Pietrzyk, M., Roucoules, C., Hodgson, P.D., 1995, Modelling the thermomechanical and microstructural evolution during rolling of a Nb HSLA steel, *ISIJ International*, 35, 531-541.

Pietrzyk, M., Kuziak, R., 1999, Coupling the thermal-mechanical finite-element approach with phase transformation model for low carbon steels, *Proc. 2nd ESAFORM Conf. on Material Forming*, ed., Covas J., Guimaraes, 525-528.

Pietrzyk, M., Kuziak, R., Kondek, T., 2003, Physical and numerical modelling of plastic deformation of steels in two-phase region, *Proc. 45th MWSP Conf*., Chicago, 209-220.

Pietrzyk, M., Madej, Ł., Węglarczyk, S., 2008, Tool for optimal design of manufacturing chain based on metal forming, *CIRP Annals*, 57, 309-312.

Scheil, E., 1935, Anlaufzeit der Austenitumwandlung, *Archiv. für Eissenhüttenwesen*, 12, 565-567.

Sellars, C.M., 1979, Physical metallurgy of hot working, in: *Hot working and forming processes*, eds. Sellars, C.M., Davies, G.J., The Metals Soc., London, 3-15.

Sellars, C.M., McTeggart, G., 1972, Hot workability, *Int. Met. Rev*., 17, 1-24.

Sellars, C.M., Whiteman, J.A., 1979, Recrystallization and grain growth in hot rolling, *Met. Sci*. 13, 187-194.

Simmons, J.P., Shen, C., Wang, Y., 2000, Phase field modeling of simultaneous nucleation and growth by explicitly incorporating nucleation events, *Scripta Materialia*, 43, 935-942.

Suehiro, M., Senuma, T., Yada, H., Sato, K., 1992, Application of mathematical model for predicting microstructural evolution to high carbon steels, *ISIJ International*, 32, 433-439.

Szeliga, D., Gawąd, J., Pietrzyk, M., 2006, Inverse analysis for identification of rheological and friction models in metal forming, *Computer Methods in Applied Mechanics and Engineering*, 195, 6778-6798.

Umemoto, M., Hiramatsu, A., Moriya, A., Watanabe, T., Nanba, S., Nakajima, N., Anan, G., Higo, Y., 1992, Computer modelling of phase transformation from work-hardened austenite, *ISIJ International*, 32, 306-315.

Waengler, S., Kawalla, R., Kuziak, R., 2008, High strength–high toughness bainitic steels alloyed with niobium for long products, steel research international, 79, spec. ed. *Metal Forming Conf*., 2, 273-279.

Zajac, S., Schwinn, V., Tacke, K.H., 2005, Characterization and quantification of complex bainitic microstructures in high and ultra-high strength linepipe steels, *Materials Science Forum*, 500-501, 387-394.

STALE BAINITYCZNE JAKO ALTERNATYWA DLA KONWENCJONALNYCH STALI WĘGLOWO-MANGANOWYCH W WYTWARZANIU ELEMENTÓW ZŁĄCZNYCH – SYMULACJA CYKLU PRODUKCJI

Streszczenie

Celem pracy jest zastosowanie komputerowego wspomagania projektowania technologii kucia elementów złącznych ze stali bainitycznych. Omówiono główne cechy stali bainitycznych nowej generacji. Opracowano modele reologiczne i modele rozwoju mikrostruktury dla wybranej stali. Modele zostały zaimplementowane w programie z metody elementów skończonych do symulacji zjawisk cieplno-mechanicznych w procesach plastycznej przeróbki metali. Szczegółowe cele pracy były dwojakie. Pierwszym zadaniem była symulacja różnych wariantów cyklu produkcji. Rozważono operacje walcowania na gorąco prętów, chłodzenia po walcowaniu, ciągnienia na zimno, wielostopniowego kucia na zimno i obróbki cieplnej. Na podstawie symulacji wybrano najlepszy cykl produkcji, dla którego wykonano próby w warunkach przemysłowych.

Submitted: May 21, 2011.
Submitted in a revised form: June 20, 2011.
Accepted: July 07, 2011.